Near-Space Wide-Swath Radar Imaging With Multiaperture Antenna

Wen-Qin Wang, *Member, IEEE*

***Abstract*—Near-space, defined as the altitude region between 20 and 100 km, offers many capabilities that are not accessible for low Earth-orbit (LEO) satellites or airplanes because it is above storm and not constrained by orbital mechanics and high fuel consumption. Hence, a high flying speed can be obtained for the maneuvering vehicles operating in near-space. This offers a promising solution to simultaneous high-resolution and wide-swath synthetic aperture radar (SAR) imaging. As such, one near-space wide-swath SAR imaging technique is presented in this letter. The system configuration, signal model, and imaging scheme are described. An example near-space SAR system is designed, and its imaging performance is analyzed. Simulation results show that near-space maneuvering vehicle SAR indeed seems to be a promising solution to wide-swath SAR imaging.**

***Index Terms*—Digital beamforming, maneuvering vehicle, multiaperture antenna, near-space, synthetic aperture radar (SAR), wide-swath imaging.**

I. Introduction

NEAR-SPACE, defined as the altitude between 20 and 100 km, was too high for conventional aircrafts but too low for low Earth-orbit (LEO) satellites [1]. Generally speaking, satellites usually operate in the orbits above 200 km, and air-breathing airplanes cannot routinely operate higher than 18 km. We thus have a gap that there are no sensors in the altitude between airplanes and satellites. Near-space offers many capabilities that are critical to emerging radar imaging techniques but not accessible from current satellites and airplanes. Near-space platform offers two obvious advantages. First, it is above the troposphere and atmosphere region where most weather conditions occur. There is a region in near-space where average winds are less than 20 knots, with peak winds being less than 45 knots 95% of the time; hence, as investigated in [2], a high velocity of 3 to 5 Mach can be achieved for near-space maneuvering vehicles. Second, it is low in cost. Near-space platform's inherent simplicity, recoverability, and no space-hardening requirements all contribute to this strong advantage. Thus, by placing radar sensors on near-space vehicles, many functions that are currently performed with satellites or airplanes could be performed cheaply.

However, a literature search in the area of near-space reveals that most work concentrates on designing near-space vehicles, including balloons and maneuvering vehicles (this letter considers only the maneuvering ones), but little work on the use of near-space sensors for communication and navigation applications has been reported. Even less effort has been placed on near-space radar imaging techniques [3], [4]. Future synthetic aperture radar (SAR) will be required to produce high-resolution imagery over a wide area of surveillance (wide-swath), but the minimum antenna area constraint makes it a contradiction [5], [6]. Consequently, current spaceborne SAR has imaging capability of wide-swath with a limited azimuth resolution. In contrast, airborne SAR has an imaging capability of high-resolution, but with a limited swath coverage. There is, therefore, a desire to increase swath coverage and azimuth resolution simultaneously [7]. As the near-space platforms considered in this letter only operate in the altitude higher than that of airplanes but lower than that of satellites with a high flying speed, compared to spaceborne and airborne SAR, simultaneous relative high-resolution and wide-swath SAR imaging is possible.

This letter presents one near-space maneuvering vehicle-based wide-swath SAR imaging technique. To suppress possible azimuth ambiguities, multiple beams in azimuth are also used. The focus is placed on presenting the system configuration, signal model, and imaging scheme. The remaining sections are organized as follows. In Section II, the presented near-space maneuvering-vehicle-based SAR is conceptually designed, followed by the ambiguity analysis in Section III. Next, an example system is designed in Section IV. This letter is concluded in Section V.

II. Conceptual Design

We consider a simplified geometry of the near-space side-looking SAR. To avoid possible range ambiguities resulting from the preceding and succeeding pulse echoes arriving at the antenna simultaneously, the slant range (R) [6] should be satisfied with [6]

$$\frac{c_o}{2}\left(\frac{n}{\mathrm{PRF}}+T_p+\Delta T_{tr}\right)<R<\frac{c_o}{2}\left(\frac{n+1}{\mathrm{PRF}}-T_p\right) \quad (1)$$

Manuscript received November 29, 2008. First version published March 04, 2009; current version published June 10, 2009. This work was supported in part by the Open Fund of the Key Laboratory of Ocean Circulation and Waves, Chinese Academy of Sciences under Contract KLOCAW0809; the Beijing Key Lab of Spatial Information Integration and 3S Application, Peking University, under Contract SIIBKL08–1-04; and the Institute of Plateau Meteorology, China Meteorological Administration, under Contract LPM2008015.

The author is with the School of Communication and Information Engineering, University of Electronic Science and Technology of China, Chengdu 610054, China, and also with the Key Laboratory of Ocean Circulation and Waves, Chinese Academy of Sciences, Qingdao 266071, China (e-mail: wqwang@uestc.edu.cn).

Color versions of one or more of the figures in this letter are available online at http://ieeexplore.ieee.org.

Digital Object Identifier 10.1109/LAWP.2009.2016584

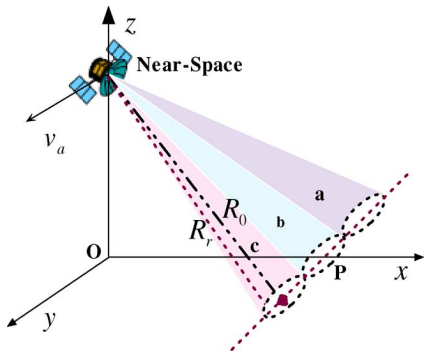

Fig. 1. Near-space wide-swath SAR using multiaperture in azimuth.

where c_o is the speed of light, n is an integer, T_p is the pulse duration, and ΔT_{tr} is the switching time between transmit and receive. The corresponding ground swath is

$$W_s \leq \frac{c_o}{2\sin(\eta)}\left(\frac{1}{\text{PRF}} - 2T_p - \Delta T_{tr}\right) \tag{2}$$

where η is the incidence angle. Substituting the expression of SAR azimuth resolution ρ_a and rearranging the terms in (2), we have

$$\frac{W_s}{\rho_a} \leq \frac{c_o}{2v_a\sin(\eta)} \tag{3}$$

where v_a is the sensor velocity. From (3) we can see that the ratio between the azimuth resolution and swath width depends on sensor velocity and incidence angle. Generally speaking, c_o/v_a is nearly constant at 20 000 for LEO satellites and typically in the range of 300 000–750 000 for airplanes. For near-space maneuvering vehicles, the c_o/v_a will be greater than 100 000. Thus, while compared to spaceborne and airborne SARs, near-space SAR can provide an optimal solution to simultaneous high-resolution and wide-swath imaging.

To further alleviate the requirements on the minimum antenna area, this letter uses multiaperture (e.g., N) in azimuth, as shown in Fig. 1. A distinct channel is associated with each subaperture, which is separately amplified, downconverted and digitized. The collected data is split according to the azimuth angular position, i.e., the instantaneous Doppler center frequency. Consequently, the minimum antenna area for each subaperture can be N times smaller than the respective antenna area, or the swath width can be N times larger than a general case. Thereafter, the displaced phase center technique [8] can be used to gain additional azimuth samples that enable an efficient azimuth ambiguity suppression. This allows the division of a broad Doppler spectrum into multiple narrow subspectra with different Doppler centroids. In this way, the whole Doppler spectrum can be recovered unambiguously by applying reconstruction filters. From the sampling theorem, we know that the sampled signal spectrum $X_s(f)$ is the sum of the

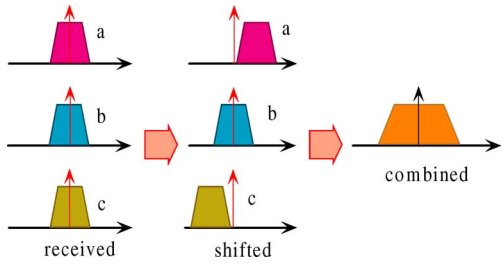

Fig. 2. Coherently combines the multiaperture spectrums.

unsampled signal spectrum, $X_0(f)$, which is repeated every f_s Hz with f_s being the sampling frequency

$$X_s(f) = f_s \sum_{n=-\infty}^{\infty} X_0(f - nf_s). \tag{4}$$

If $f_s \geq 2B_{ds}$ where B_{ds} is the Doppler bandwidth, then the replicated spectra do not overlap, and the original spectrum can be regenerated by chopping $X_s(f)$ off above $f_s/2$. Thus, $X_0(f)$ can be reproduced from $X_s(f)$ through an ideal low-pass filter that has a cutoff frequency of $f_s/2$.

Finally, in a manner similar to adaptive antenna beamforming technique [9], the filtered signals can be combined coherently, as shown in Fig. 2. In this way, each subaperture antenna can operate at a lower pulsed repeated frequency. Note that to obtain optimum performance, the relation between sensor velocity and the along-track offsets of each subchannel has to result in equally spaced effective phase centers so a uniform sampling of the received signal can be obtained.

III. Ambiguity Analysis

For a given PRF or range of the PRFs, the antenna dimensions must be satisfied with the required ambiguity-to-signal ratio specification. Azimuth ambiguities arise from finite sampling of the Doppler signal. As the azimuth spectrum repeats at an interval of the PRF, the signal components outside this frequency interval will be folded back into the main part of the spectrum, as shown in Fig. 3. Consequently the desired signals will be contaminated by the ambiguous signals from adjacent spectra. This can be evaluated by the azimuth ambiguity-to-signal ratio (AASR) defined as [10]

$$\text{AASR} \approx \frac{\sum_{\substack{m=-\infty \\ m\neq 0}}^{\infty} \int_{-0.5B_d}^{0.5B_d} G^2(f + m\cdot\text{PRF})df}{\int_{-0.5B_d}^{0.5B_d} G^2(f)df} \tag{5}$$

where B_d and $G(f)$ denote the processing bandwidth and antenna pattern in azimuth, respectively.

Considering the three subapertures illustrated in Fig. 1, we have

$$G_k(\theta) = \text{sinc}^2\left(\frac{\pi L_{as}\cos(i\cdot\theta_s)}{\lambda}\sin(\alpha - i\cdot\theta_s)\right)$$
$$i \in (-1, 0, 1), k \in (a, b, c) \tag{6}$$

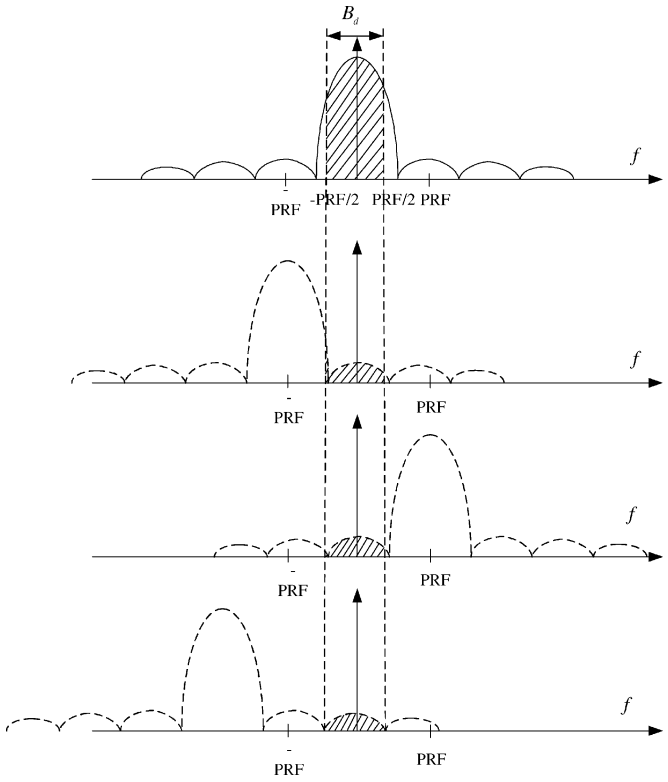

Fig. 3. Illustration of SAR azimuth ambiguities.

where α is the off-axis angle, and θ_s and L_{as} are the beamwidth and antenna length in azimuth for each subaperture, respectively. Note that $i \in (-1, 0, 1)$ is accordingly determined from the positions of the three subapertures a, b, c, i.e., $i = -1$ for a , $i = 0$ for b, and $i = 1$ for c. The 3-dB beamwidth is approximately determined by [10]

$$\alpha \approx \frac{\lambda}{2v_a} f, \qquad \theta_s = k_a \frac{\lambda}{L_{as}} \tag{7}$$

where $k_a \leq 1$ is a given constant. Equation (6) can then be further simplified into

$$G_k(f) \approx \operatorname{sinc}^2 \left[\pi L_{as} \cos\left(i \cdot \frac{k_a c_0}{f L_{as}} \right) \left(\frac{f}{2v_a} - i \cdot \frac{k_a}{L_{as}} \right) \right] \quad i \in (-1, 0, 1). \tag{8}$$

Then, from (5) we can get (9), shown at the bottom of the page.

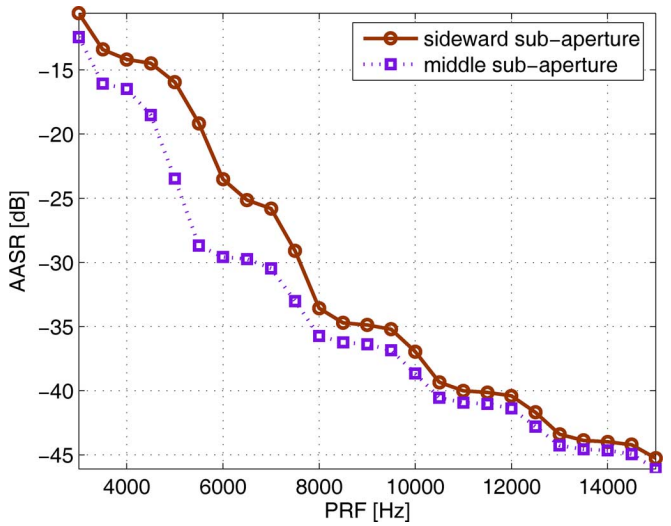

Fig. 4. The AASR of an example near-space SAR as a function of PRF.

As an example, consider a near-space SAR with the following parameters: $H_0 = 20$ km, $v_a = 500$ m/s, $\lambda = 0.03$ m, $L_{as} = 0.4$ m The AASR is illustrated in Fig. 4. Note that AASR is typically specified to be on the order of -20 dB, but a lower AASR is desirable.

Similarly, range ambiguities may result from preceding and succeeding pulse echoes arriving at the antenna simultaneously. This type of ambiguity is relatively not significant for near-space SAR. The range ambiguity of the near-space wide-swath SAR discussed in this letter can be analyzed in a manner similar to the general SAR. The PRF is, therefore, designed by the maximum acceptable range and azimuth ambiguity-to-signal ratios as well as the transmit and nadir interference [11]. Note that, there may be no acceptable PRFs at some incidence angles that meet the minimum requirements. The designer then has the option to relax the performance specifications for this imaging area or exclude it from the operation plan.

IV. An Example Near-Space Wide-Swath SAR

To manifest the imaging performance, an example near-space wide-swath SAR is designed in this section. It operates in the x-band with a center frequency of 10 GHz. A quantity directly related to SAR processing is the noise equivalent sigma zero (NESZ) defined as the radar cross-section (RCS) for which the signal-to-noise ratio (SNR) is equal to 1 (SNR= 0 dB). The

$$\mathrm{AASR}_k(\mathrm{PRF}) = \left\{ \sum_{\substack{m=-\infty \\ m\neq 0}}^{\infty} \left[\int_{(i-0.5)B_{ds}}^{(i+0.5)B_{ds}} G_k^2(f + m \cdot \mathrm{PRF}) df + \sum_{j \neq k} \int_{(i-0.5)B_{ds}}^{(i+0.5)B_{ds}} G_k(f + m \cdot \mathrm{PRF}) G_j(f + m \cdot \mathrm{PRF}) df \right] \right\} \cdot \left\{ \int_{(i-0.5)B_{ds}}^{(i+0.5)B_{ds}} G_k^2(f) df + \sum_{j \neq k} \int_{(i-0.5)B_{ds}}^{(i+0.5)B_{ds}} G_k(f) G_j(f) df \right\}^{-1}, \quad k, j \in (a, b, c),\ i \in (-1, 0, 1). \tag{9}$$

TABLE I
PERFORMANCE PARAMETERS OF AN EXAMPLE NEAR-SPACE SAR

Parameters	Variables	Values
mean transmit power	P_{avg}	$1W$
number of sub-aperture	N	3
sub-aperture antenna length	L_{as}	$0.40m$
sub-aperture antenna width	H_a	$0.10m$
near-space vehicle velocity	v_s	$500m/s$
incidence angle	η	20°
swath width	W_s	$6.80km$
radiometric resolution	$NESZ$	$-48.58dB$
incidence angle	η	25°
swath width	W_s	$7.30km$
radiometric resolution	$NESZ$	$-48.11dB$
incidence angle	η	35°
swath width	W_s	$8.94km$
radiometric resolution	$NESZ$	$-46.73dB$

NESZ can also be interpreted as the smallest target RCS that is detectable by the SAR against thermal noise. From the radar equation, we obtain [12]

$$\mathrm{NESZ} = \frac{8\pi R_s^3 v_s \lambda K T_{\mathrm{sys}} F_n L_f}{P_{\mathrm{avg}} N A_{as}^2 \rho_r} \tag{10}$$

where R_s is the average slant range that is assumed constant in this letter, K ($K \approx 1.38 \times 10^{-23}$) is the Boltzmann constant, T_{sys} is the system noise temperature, L_f is the loss factor, F_n is the receiver noise figure, P_{avg} is the average transmit power, N is the number of subaperture (defined previously), A_{as} is the subaperture antenna area, and ρ_r is the range resolution cell for one look.

To calculate the system performance, we assume a range resolution $\rho_r = 0.2$ m, an overall loss factor $L_f = 3$ dB, and a receiver noise figure of $F_n = 3$ dB. It is further assumed that the signal bandwidth is adjusted for varying incidence angle such that the ground-range resolution is constant across the whole swath. An example system design is provided in Table I. We note that, for the incidence angle given in Table I, the swath width is about 8 km and the NESZ is approximately -48 dB. These results show that a satisfactory performance can be achieved, however, with only a small number of subaperture with relative small antenna area. The conclusion is that unambiguous range and swath width can be obtained using a near-space SAR with multiaperture in azimuth.

V. CONCLUSION

This letter proposes one near-space maneuvering vehicle-based high-resolution and wide-swath SAR imaging technique. We do not advocate eliminating satellites and airplanes; however, near-space vehicles indeed are the best choice for high-resolution and wide-swath SAR imaging. One remaining problem is interbeam suppression because multiple apertures are used in this letter [13], [14]. A possible solution is the use of waveform diversity to provide some cross-cancellation of data in different subapertures [15]. Another problem is motion compensation because near-space SAR cannot take complex motion measurement sensors due to its limited load capability. One possible solution to use the transponder to extract the motion errors [16].

ACKNOWLEDGMENT

The author would like to thank the editor and referees for their helpful comments.

REFERENCES

[1] E. B. Tomme, "Balloons in today's military: An introduction to the near-space concept," *Air Space. J.*, vol. 19, no. 4, pp. 39–50, 2005.
[2] E. B. Tomme, "The paradigram shift to effects-based space: Near-space as a combat space effects enabler," 2008 [Online]. Available: http://www.airpower.au.af.mil
[3] M. Galletti, G. Krieger, B. Thomas, M. Marquart, and S. S. Johannes, "Concept design of a near-space radar for tsunami detection," in *Proc. IEEE Geosci. Remote Sens. Symp.*, Barcelona, Spain, Jun. 2007, pp. 34–37.
[4] W. Q. Wang, "Application of near-space passive radar for homeland security," *Sens. Imag.: An Int. J.*, vol. 8, no. 1, pp. 39–52, Mar. 2007.
[5] Z. F. Li, H. Y. Wang, T. Su, and Z. Bao, "Generation of wide-swath and high-resolution SAR images from multichannel small spaceborne SAR systems," *IEEE Geosci. Remote Sens. Lett.*, vol. 2, no. 1, pp. 82–86, Jan. 2005.
[6] A. Currie and M. A. Brown, "Wide-swath SAR," *IEE Radar Signal Process.*, vol. 139, no. 2, pp. 122–135, Apr. 1992.
[7] R. W. Linderman, "Swathbuckler: Wide swath SAR system architecture," in *Proc. IEEE Radar Conf.*, New York, Apr. 2006, pp. 1–6.
[8] C. E. Muehe and M. Labitt, "Displaced-phase-center antenna technique," *Lincoln Lab. J.*, vol. 12, no. 2, pp. 281–296, Jun. 2000.
[9] S. R. Miller and A. Spanias, "Adaptive antenna beamforming using quiescent pattern control," *IEEE Antenna Wireless Propag. Lett.*, vol. 6, pp. 651–654, 2007.
[10] F. K. Li and W. T. K. Johnson, "Ambiguities in spaceborne synthetic aperture radar systems," *IEEE Trans. Aerosp. Electron. Syst.*, vol. AES-19, pp. 389–397, May 1983.
[11] K. T. Selvan, "Accurate design method for pyramidal horns of any desired gain and aperture phase error," *IEEE Antenna Wireless Propag. Lett.*, vol. 7, pp. 31–32, 2008.
[12] G. Selvan and A. Moreira, "Spaceborne bi- and multi-static SAR: Potential and challenges," *IEE Proc. Radar, Sonar Navig.*, vol. 153, no. 3, pp. 184–198, Jun. 2006.
[13] J. A. Hejres, A. Peng, and J. Hijres, "Fast method for sidelobe nulling in a partially adaptive linear array using the elements positions," *IEEE Antenna Wireless Propag. Lett.*, vol. 6, pp. 332–335, 2007.
[14] C. Hertleer, A. Tronquo, H. Rogier, L. Vallozzi, and L. Van. Langenhove, "Aperture-coupled patch antenna for integration into wearable textile systems," *IEEE Antenna Wireless Propag. Lett.*, vol. 6, pp. 392–395, 2007.
[15] W. Q. Wang, Q. C. Peng, and J. Y. Cai, "Waveform-diversity-based millimeter-wave UAV SAR remote sensing," *IEEE Trans. Geosci. Remote Sens.*, vol. 47, no. 3, pp. 691–700, 2009.
[16] W. Q. Wang, "Inflight antenna pattern measurement for bistatic synthetic aperture radar systems," *IEEE Antenna Wireless Propag. Lett.*, vol. 6, pp. 432–435, 2007.